Electron exchange energy of neutral donors inside a quantum well

G. Garcia-Arellano, F. Bernardot, C. Testelin, and M. Chamarro
Sorbonne Université, CNRS, Institut des NanoSciences de Paris, 4 place Jussieu, F-75005 Paris, France

(Received 24 July 2018; revised manuscript received 15 October 2018; published 19 November 2018)

We calculated the exchange energy of a pair of donor-bound electrons placed in the middle of an infinite quantum well (QW). In order to obtain this energy for any interdonor distance and for any QW thickness, we have first adapted to a QW the method developed by Gor'kov and Pitaevskii [L. P. Gor'kov and L. P. Pitaevskii, Dokl. Akad. Nauk SSSR **151**, 822 (1963)] for a three-dimensional (3D) distribution of donors, and calculated the asymptotic form of the exchange energy. Second we have calculated the exchange energy of a "helium atom" in a QW; and third, inspired by the interpolation procedure proposed by Ponomarev *et al.* [I.V. Ponomarev *et al.*, Phys. Rev. B **60**, 5485 (1999)], we have obtained an interpolated expression for any interdonor distance. The obtained exchange energy is written in units of effective hartree, and the distance between the donors, as well as the width of the QW, are expressed in units of effective Bohr radius. We calculated the exchange energy for some commonly studied semiconductor materials, and discussed also the relationship between the exchange energy and the spin relaxation time for a donor concentration close to the insulator-metal transition.

DOI: 10.1103/PhysRevB.98.195308

I. INTRODUCTION

The association of the carrier-carrier Coulomb interaction and the antisymmetric character of the state of an electron pair are at the foundation of the exchange interaction between localized electrons; this interaction is one of the oldest topics in quantum mechanics. In the last decade, the strong interest in controlling and manipulating localized spins in solid-state systems, such as quantum dots or impurities, has renewed this topic. Indeed, since the birth of the idea of a quantum computer [1,2] numerous efforts, both theoretical and experimental, have been made to physically identify qubit candidates. Solid-state qubits are a subset of qubits which present the advantage of scalability due to the use of nanofabrication technologies, but which also present challenges to obtain a suitable protection against interactions from their environment. Another issue is to fabricate qubits identical to each other, and to make them properly communicate. Nowadays, the two main qubit technologies concern superconductor and semiconductor materials, for which several qubits have been identified. In superconducting circuits obtained with nanotechnologies similar to those of the microelectronics, qubits based on phase, charge of flux states have reached a spectacular degree of quantum control [3,4]. One of the main requirements for qubits is to show long coherence times, and then in solid-state physics these qubits have to be protected against environmental interactions. In this sense, the spin of the low-energy electronic states in semiconductors is, in principle, an observable well protected from the environment, and constitutes a good prototype of a qubit. Moreover, to suppress the relaxation mechanism of itinerant electrons (D'yakonov-Perel process), the electron spin should be localized at a nanometer scale. The confinement can be obtained by nanofabrication as in quantum dots [5–8], or in a more natural way using the attractive potential of individual impurities [9–13]. Some years ago, electrons trapped by individual donors in semiconductors at low temperature emerged as one of the possible candidates [8,14–17]. In particular, it has been experimentally demonstrated that, when donors are immersed in a quantum well (QW), the spin relaxation time of electrons localized on donors enhances by two orders of magnitude with respect to spin relaxation time of free electrons in QWs [18]. Moreover, by inserting the donors in a QW, the optical selection rules for circularly polarized light are purified, allowing a higher degree of optical orientation of the electron spins than in 3D crystals [18–21].

In this framework, two main challenges are related with the exchange energy between spin qubits: (i) the enhancement of the relaxation and coherence times, and (ii) the mechanism of the entanglement in a pair of qubits. The spin relaxation time is strongly related to the distance between two electrons localized on donors. Several experimental and theoretical studies have addressed this issue [12,22–24]. Different mechanisms contribute to the spin relaxation: at very low concentration of donors, the coupling of an isolated electron spin with the surrounding nuclear spins is the dominant interaction, and at donor concentrations near the metallic transition the exchange interaction is the main mechanism of the spin-spin interaction between neighboring donors. Controlled entanglement requires a well-known interaction between spin qubits, the strength of which fixes the speed of a two-qubit gate. Different mechanisms of entanglement have been proposed, as for example coupling to photons *via* a cavity mode [25,26], coupling to virtual excitations of delocalized exciton states [27], dipole-dipole interaction between charged excitons strongly polarized by an external dc field [28], or the exchange interaction between two electrons in neighboring qubits [8,9,29].

The most appropriate method to get the exchange energy in the limit of large distances between donors was developed by Gor'kov and Pitaevskkii, and Herring and Flicker [30,31]. In this method, the authors calculated the exchange energy between two "hydrogen atoms", reducing its expression to a hyperplane integral in a six-dimensional space, and finally

getting an analytical formula in 3D. Later, Ponomarev *et al.* [32] proposed a procedure to obtain an expression valid for any interdonor distance. This procedure is based on an interpolation between the exchange energy at zero distance (i.e., the "helium atom") and the known asymptotic behavior. The same authors also calculated the asymptotic and interpolated exchange energies for artificial two dimensional (2D) systems: electrons confined to the same plane as the impurities, and electrons bound to Coulomb centers which are located outside the plane [33].

In this paper, we have calculated the exchange energy of a pair of donor-bound electrons placed in the middle of an infinite QW, for any interdonor distance and for different QW thicknesses. We calculated first, in Sec. II, the asymptotic form of the exchange energy, adapting to a QW the method developed in Refs. [30,31]. In Sec. III, inspired by the interpolation procedure proposed by Ponomarev *et al.* [32], we calculated the exchange energy of a "helium atom" inside an infinite QW, and finally reached the values of the exchange energy valid for any interdonor distance and for any QW thickness. In Sec. IV, we discussed the behavior of the exchange energy in different III-V and II-VI materials, and its relationship with the spin relaxation time at donor concentrations close to the insulator-metal transition.

II. EXCHANGE ENERGY FOR LARGE DISTANCES BETWEEN DONORS

A. General framework

We consider two electrons, 1 and 2, localized at low temperature on two donors A and B. Both donors are located at fixed positions $x_A = -a$ and $x_B = +a$ in a semiconductor matrix. The Hamiltonian describing the system of both donor-bound electrons is

$$\widehat{H} = -\frac{\Delta_1}{2} - \frac{\Delta_2}{2} - \frac{1}{r_{1A}} - \frac{1}{r_{2B}} - \frac{1}{r_{1B}} - \frac{1}{r_{2A}} + \frac{1}{r_{12}} + \frac{1}{2a}, \tag{1}$$

where Δ_j is the Laplacian operator acting on electron j ($j =$ 1 or 2), r_{jA} and r_{jB} are the distances of electron j to donors A and B, respectively, and $r_{12} = |\vec{r}_2 - \vec{r}_1|$ is the distance between the electrons. In the following, the Cartesian coordinates x_j, y_j, z_j of electron j ($j = 1$ or 2) will be employed. Here, and in the following, the distances are expressed in units of effective (bulk) Bohr radius a_B^*, and the energies in units of effective hartree E_h^*; a_B^* and E_h^* are defined as follows: $a_B^* = a_0\varepsilon_r(m/m^*)$, with $a_0 = 4\pi\varepsilon_0\hbar^2/me^2 \approx 0.52918$ Å the Bohr radius of the atomic units, and $E_h^* = E_h(m^*/m\varepsilon_r^2)$, where $E_h = e^2/4\pi\varepsilon_0 a_0 \approx 27.211$ eV is the hartree energy of the atomic units; m is the electron mass, m^* the effective electron mass, and ε_r the dielectric constant.

The Hamiltonian $\hat{H}$ being independent on the electron spins $\vec{S}_1$ and $\vec{S}_2$, the Pauli principle implies that the two-electron states are singlet states $\Psi = \Psi_S|S = 0, S_z = 0\rangle$, with an orbital part Ψ_S symmetric by electron exchange $[\Psi_S(\vec{r}_2, \vec{r}_1) = +\Psi_S(\vec{r}_1, \vec{r}_2)]$, or triplet states $\Psi = \Psi_A|S = 1, S_z = 0, \pm 1\rangle$, with an orbital part Ψ_A antisymmetric by electron exchange $[\Psi_A(\vec{r}_2, \vec{r}_1) = -\Psi_A(\vec{r}_1, \vec{r}_2)]$; $\vec{S} = \vec{S}_1 + \vec{S}_2$ is the total spin of the pair of electrons. As it is well know that the ground state of such a system is a singlet and the first-excited one a triplet, the notations Ψ_S and E_S designate from now on the wavefunction and energy of the ground state, and Ψ_A and E_A the ones of the first-excited state.

The energy difference between the first-excited and the ground levels, $E_A - E_S = 2J$, is called the *exchange energy*, or *exchange splitting*, of the two-electron system. We are using here, and in all the following, a positively defined exchange energy, $2J > 0$: the Hamiltonian $\hat{H}$ of Eq. (1) then corresponds to the spin Hamiltonian $\hat{H}_{\rm exc} = +2J\ \vec{S}_1 \cdot \vec{S}_2$. Let us stress that the spin-orbit interaction, not taken into account in Eq. (1), brings additional anisotropic contributions in $\hat{H}_{\rm exc}$, see Refs. [24,34]. We do not write them here, because we are concerned by the isotropic part of $\hat{H}_{\rm exc}$; they are considered in Sec. IV.

The calculation of the exchange energy $2J$, in the limit of large distances $R = 2a$ between donors, was first explored in the 1920's [35]. A more refined, and more correct, method was later developed in Refs. [30,31] for doped bulk materials (3D case), and also used in the purely 2D case (see Refs. [32,33]) of two donors placed in a plane. This latter method yields an integral expression of the exchange energy:

$$2J(R \gg 1) = \int_\Sigma \Psi_2 \vec{\nabla} \Psi_1 . d\Sigma, \tag{2}$$

with $\Psi_1 = \Psi_S + \Psi_A$ and $\Psi_2(\vec{r}_1, \vec{r}_2) = \Psi_1(\vec{r}_2, \vec{r}_1)$, the integral being on the hyperplane Σ defined by $x_2 = x_1$, and the elemental hypersurface $d\vec{\Sigma}$ pointing towards the $x_2 > x_1$ region. At this stage, Ψ_1 can be approximated in Eq. (2) by the expression

$$\Psi_1(\vec{r}_1, \vec{r}_2) = \phi_A(\vec{r}_1)\phi_B(\vec{r}_2)\chi(\vec{r}_1, \vec{r}_2), \tag{3}$$

where $\phi_A(\vec{r}) = \phi_1(\vec{r} - \vec{R}_A)$ is the one-electron ground-state wavefunction on donor A, located at $\vec{R}_A$, $\phi_B(\vec{r}) = \phi_1(\vec{r} - \vec{R}_B)$ is the one for donor B, located at $\vec{R}_B$, and $\chi(\vec{r}_1, \vec{r}_2)$ is a slowly varying correlation function manifesting that the two electrons are avoiding each other: $\chi(\vec{r}_1, \vec{r}_2) = 0$ for $\vec{r}_1 = \vec{r}_2$. The χ function is first determined, and so the calculations in 3D and 2D have been achieved by inserting expression (3) in Eq. (2), see Eqs. (10).

B. Calculation in an infinite quantum well

The case of two donors placed in the mid-plane $z = 0$ of an infinite QW, of thickness L, introduces an extrinsic confinement of the 3D one-electron wavefunctions. This situation is intermediate between those at 3D and 2D, with L as a variable parameter. Here, we employed the one-electron ground-state wavefunction $\phi_1(\vec{r})$ studied in Appendix A, with atomic number $Z = 1$. Then, following the steps of the method developed to reach $2J(R \gg 1)$ in 3D (Ref. [30]), it turns out that the function $\chi(\vec{r}_1, \vec{r}_2)$ obeys the equation

$$\alpha_1\left(\frac{\partial\chi}{\partial x_1} - \frac{\partial\chi}{\partial x_2}\right) + \left(\frac{1}{2a} + \frac{1}{r_{12}} - \frac{1}{a - x_1} - \frac{1}{a + x_2}\right)\chi = 0, \tag{4}$$

considering the positions of both electrons near the x axis, with $x_1 > -a$ and $x_2 < a$; α_1 is the radial decreasing rate of ϕ_1 (see Appendix A) – in 3D, $\alpha_1 = 1$ –. So it appears that

the function χ^{α_1} obeys the equation met in 3D. Considering the limit conditions $\chi \to 1$ when $x_1 \to -a$ or $x_2 \to a$, this means that χ^{α_1} coincides with the 3D correlation function χ_{3D}. Using the known expression of $\chi_{3D}(\vec{r}_1, \vec{r}_2)$, see Ref. [30] or Appendix D, we hence deduced

$$\chi(\vec{r}_1, \vec{r}_2) = \chi_{3D}(\vec{r}_1, \vec{r}_2)^{1/\alpha_1}. \tag{5}$$

Noticeably, this expression of $\chi(\vec{r}_1, \vec{r}_2)$ goes to the right 3D limit [30] when $\alpha_1 \to 1$ (for $L \to \infty$), and also to the right 2D limit [32,33] when $\alpha_1 \to 2$ (for $L \to 0$).

We are now able to express the exchange energy $2J(R \gg 1)$ in its integral form (2). Retaining only derivatives of ϕ_1 with respect to x_1 and x_2, and neglecting the terms containing the derivatives of χ, we are first conducted to

$$2J = 8\alpha_1 \int_0^a dx_1 \int_{-\infty}^{+\infty} dy_1 dy_2 \times \int_{|z_{1,2}|<L/2} dz_1 dz_2 \, \Psi_1(\vec{r}_2, \vec{r}_1)|_{x_2=x_1} \Psi_1(\vec{r}_1, \vec{r}_2)|_{x_2=x_1}, \tag{6}$$

and then to

$$2J(R \gg 1) = 4\,\alpha_1 \left(\frac{8}{\mathrm{e}}\right)^{\frac{1}{\alpha_1}} {A_1}^4 \, R^{3-\frac{1}{2\alpha_1}} \, \mathrm{e}^{-2\alpha_1 R} \int_0^1 dX \times \int_{|Z_{1,2}|<\frac{L}{2\sqrt{R}}} dZ_1 dZ_2 \int_{-\infty}^{+\infty} dY_1 dY_2 \times \cos^2\left(\frac{\pi\sqrt{R}Z_1}{L}\right)\cos^2\left(\frac{\pi\sqrt{R}Z_2}{L}\right) \times \exp\left\{-\frac{2\alpha_1\left(P_1^2+P_2^2\right)}{1-X^2} + \frac{X}{\alpha_1}\right\} \times \left[\frac{P_{12}}{(1+X)^2(1-X)}\right]^{\frac{1}{\alpha_1}}, \tag{7}$$

using $R = 2a$, the change of variables $x_1 = aX$, $y_{1,2} = Y_{1,2}\sqrt{R}$, $z_{1,2} = Z_{1,2}\sqrt{R}$, and the notations $P_j = \sqrt{Y_j^2 + Z_j^2}$ ($j = 1$ or 2) and $P_{12} = \sqrt{(Y_1 - Y_2)^2 + (Z_1 - Z_2)^2}$.

The expression (7) of the exchange energy $2J(R \gg 1)$ can be calculated numerically, for given values of the thickness L of the QW (for a given L, α_1 and A_1 are known, see Appendix A). In order to decrease the numerical integration time, we turned the 5-dimensional integral (7) to a 4-dimensional one, using the change of variables

$$S_1 = \frac{Y_1 + Y_2}{2}, \quad S_2 = \frac{Z_1 + Z_2}{2}, \quad D_1 = Y_1 - Y_2, \quad D_2 = Z_1 - Z_2; \tag{8}$$

the integration over variable S_1 can be performed, and we finally used the following expression (9) for our numerical calculations:

$$\begin{aligned} 2J(R \gg 1) = {} & 4\sqrt{\pi\alpha_1}\left(\frac{8}{\mathrm{e}}\right)^{\frac{1}{\alpha_1}} {A_1}^4 \, R^{3-\frac{1}{2\alpha_1}} \, \mathrm{e}^{-2\alpha_1 R} \int_0^1 dX \sqrt{1-X^2}\left[\frac{\mathrm{e}^X}{(1+X)^2(1-X)}\right]^{\frac{1}{\alpha_1}} \\ & \times \int_0^{+\infty} dD_1 \int_0^{\frac{L}{\sqrt{R}}} dD_2 \left(D_1^2 + D_2^2\right)^{\frac{1}{2\alpha_1}} \exp\left[-\frac{\alpha_1\left(D_1^2+D_2^2\right)}{1-X^2}\right] \\ & \times \left\{ \cos^2\left(\frac{\pi\sqrt{R}D_2}{L}\right) \int_0^{\frac{L}{2\sqrt{R}}-\frac{D_2}{2}} dS_2 \exp\left[-\frac{4\alpha_1 S_2^2}{1-X^2}\right] \right. \\ & + 2\cos\left(\frac{\pi\sqrt{R}D_2}{L}\right) \int_0^{\frac{L}{2\sqrt{R}}-\frac{D_2}{2}} dS_2 \cos\left(\frac{2\pi\sqrt{R}S_2}{L}\right) \exp\left[-\frac{4\alpha_1 S_2^2}{1-X^2}\right] \\ & \left. + \int_0^{\frac{L}{2\sqrt{R}}-\frac{D_2}{2}} dS_2 \cos^2\left(\frac{2\pi\sqrt{R}S_2}{L}\right) \exp\left[-\frac{4\alpha_1 S_2^2}{1-X^2}\right] \right\}. \end{aligned} \tag{9}$$

It is easy to check that, when $L \to \infty$ or $L \to 0$, Eq. (9) goes to the formulas known in 3D or 2D, respectively (see Refs. [31–33]):

$$2J_{3D}(R \gg 1) = 1.6366\, R^{5/2}\, \mathrm{e}^{-2R}; \tag{10a}$$

$$2J_{2D}(R \gg 1) = 30.413\, R^{7/4}\, \mathrm{e}^{-4R}. \tag{10b}$$

Figure 1 shows the exchange energy $2J(R \gg 1)$ as a function of the distance $R = 2a$ between the pair of donors, for several values of the QW thickness L. The $2J$ values for $R \sim 1$, and below, have *a priori* no physical significance, because we fixed $R \gg 1$ from the start.

III. DETERMINATION OF $2J(R)$ FOR ANY R

A. Procedure to get an interpolated expression of $2J(R)$

In Ref. [32], a procedure is proposed to build the exchange energy $2J(R)$ for any value of the distance R between the donors, in the 3D and 2D cases. This procedure makes use of (i) the asymptotic form of the exchange energy

$$2J(R \gg 1) = C R^{\beta} \mathrm{e}^{-\omega R}, \tag{11}$$

followed at 3D and 2D, see Eqs. (10); (ii) the value of the exchange energy $2J_0 = 2J(R = 0)$ of the 3D and 2D helium atom; and (iii) two analytical assumptions: $\ln[2J(R \ll 1)]$

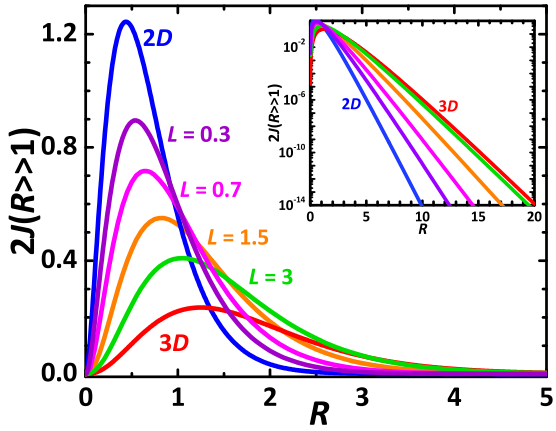

FIG. 1. Exchange energy $2J(R \gg 1)$ for several values of the QW thickness L, as a function of the distance R between two donor-bound electrons, centered inside the QW. The curves noted 2D and 3D correspond to the $L \to 0$ and $L \to \infty$ limits, respectively. Inset: semilogarithmic representation of the same data, for a larger range of R.

can be expanded as $\ln(2J_0) - \gamma R - \tilde{A}R^2 \cdots$, with γ and $\tilde{A}$ both positive, and the second derivative of $\ln[2J(R)]$ is Lorentzian for any distance R:

$$\frac{d^2 \ln[2J(R)]}{dR^2} = -\frac{2\tilde{A}\beta}{\beta + 2\tilde{A}R^2}. \tag{12}$$

A first integration of Eq. (12) gives the expression of the first derivative of $\ln[2J(R)]$ for any R, and a relationship between γ and $\tilde{A}$:

$$A = \sqrt{2\tilde{A}/\beta} = \frac{2(\omega - \gamma)}{\pi\ \beta}. \tag{13}$$

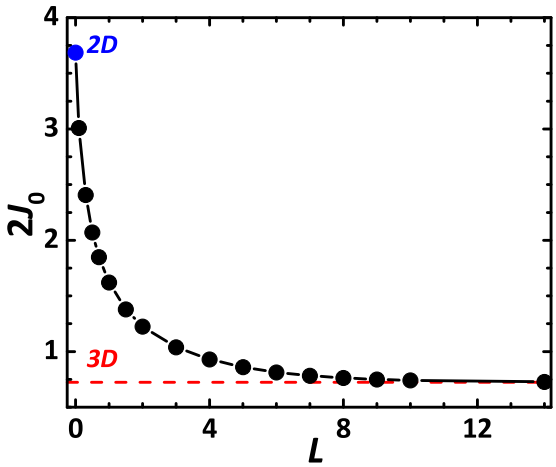

FIG. 2. Exchange energy $2J_0$ of a "helium atom" (full disks) centered in an infinite QW, as a function of the QW thickness L. The blue point at $L = 0$ corresponds to our calculated $2J_0$ in 2D; the red dashed horizontal line indicates the value of our calculated $2J_0$ in 3D (continuous curve: guide for the eyes).

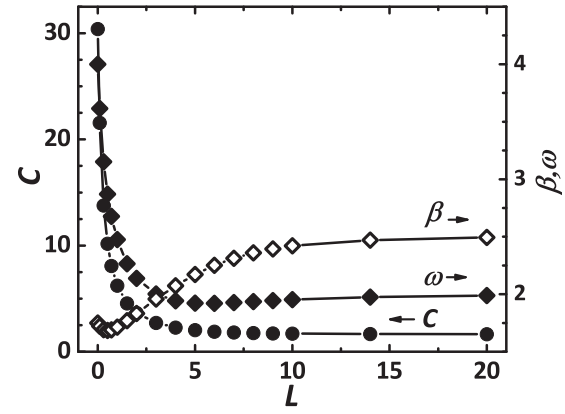

FIG. 3. Fitting parameters C (full disks), β (open diamonds), and ω (full diamonds) of the exchange energy $2J(R \gg 1)$ with Eq. (11), as a function of the QW thickness L. The values of C read on the left axis, the values of β and ω on the right axis (continuous curves: guides for the eyes).

Then, a second integration yields the interpolated formula for $2J(R)$ given by this procedure:

$$\ln[2J(R)] = \ln(2J_0) - \gamma R - \beta A R \arctan(AR) + \frac{\beta}{2}\ln(1 + A^2R^2). \tag{14}$$

One single parameter, A (or γ), remains to be determined. In Ref. [32], the authors have chosen the parameter A by fitting at best numerical values of $2J$ obtained for R of the order of unity or several units. So they proposed interpolated formulas for $2J(R)$ in the 3D and 2D cases, using a $2J_0$ value in 3D known at their time and, at 2D, a value of $2J_0$ calculated by their own. In Appendix C, we propose slightly modified expressions of $2J(R)$ for the 3D and 2D cases.

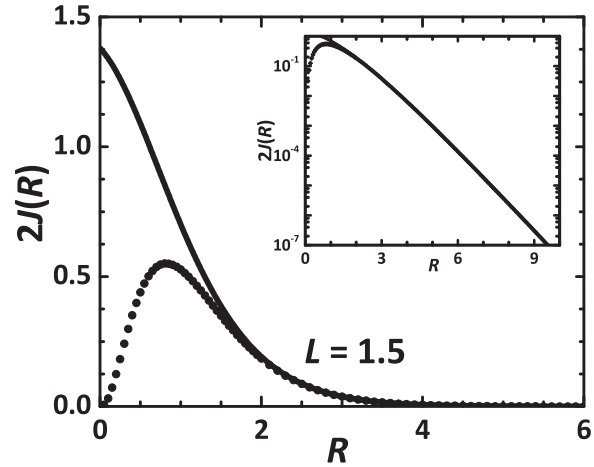

FIG. 4. Interpolated $2J(R)$ (continuous curve) and large-R $2J(R \gg 1)$ (dotted curve) exchange energies for the QW thickness $L = 1.5$, as a function of the distance R between two donor-bound electrons, centered inside the QW. Inset: semilogarithmic representation of the same data, for a larger range of R.

B. Interpolated $2J(R)$ in an infinite quantum well

In the present study of the exchange energy between two donors located in the middle of an infinite QW, we faced two issues in order to build an interpolated $2J(R)$ with the procedure described in Sec. III A: (i) the calculation of $2J_0$ in a "helium atom" centred in the QW; (ii) the creation of the interpolated $2J(R)$ starting with an asymptotic $2J(R \gg 1)$, Eq. (9), which does *not* possess the standard form (11).

Let us first discuss the calculations we made to obtain $2J_0$ in the middle of an infinite QW. We noticed that, in 3D and in 2D, calculating the ground energy E_S of the helium atom using the variational method, and the first-excited energy E_A perturbatively, gives a very good approximation of the exchange energy $2J_0$, which is found to be shifted from the exact numerical values by only about 1% (see Appendix B). So we proceeded in the same way to calculate the exchange energy of a "helium atom" located in the midplane of an infinite QW; our calculations of E_S and E_A are presented in Appendix B. Figure 2 shows $2J_0$ as a function of the thickness L of the QW; as it is observed, $2J_0$ decreases monotonously with L, from the 2D value to the 3D one.

Let us now turn to the construction of the interpolated $2J(R)$ in an infinite QW. The calculated asymptotic values of the exchange energy $2J(R \gg 1)$, see Eq. (9) and Fig. 1, do not possess exactly the form (11) met in the 3D and 2D cases. But we realized that the fit of $2J(R \gg 1)$ with Eq. (11) is rather satisfactory for values of R ranging from $R = 0.1$ to 30; the largest considered distance $R = 30$ between the two donors corresponds to residual concentrations in typical semiconductors. Then we obtained the parameters C, β, and ω which are shown in Fig. 3; we reached them by adjusting $\ln[2J(R \gg 1)]$ with $\ln C + \beta \ln R - \omega R$. Figure 3 shows these parameters as a function of the thickness of the QW. Finally, we performed a fit of the values of $2J(R \gg 1)$ between $R = 20$ and 30 with Eq. (14), using the known values of $2J_0$ and β; A was the only fitting parameter [γ is linked to A, once β and ω are fixed, see Eq. (13)]. We created in this way an interpolated formula for $2J(R)$ inside an infinite QW, for any distance R of interest between the pair of donors. An example of interpolated exchange energy $2J(R)$ is given in Fig. 4, for $L = 1.5$; its coincidence with the asymptotic form $2J(R \gg 1)$ occurs for $R \geqslant 2$.

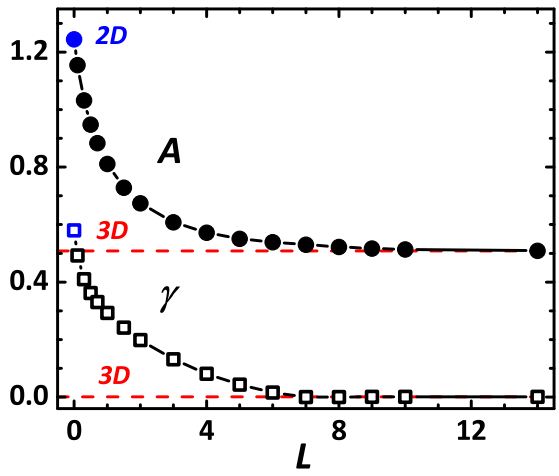

FIG. 5. Parameters A (full disks) and γ (open squares) entering in the expression of the interpolated $2J(R)$ exchange energy, see Eq. (14), as a function of the QW thickness L (continuous curves: guides for the eyes). The blue points at $L = 0$ correspond to the 2D case; the red dashed horizontal lines indicate the values in 3D.

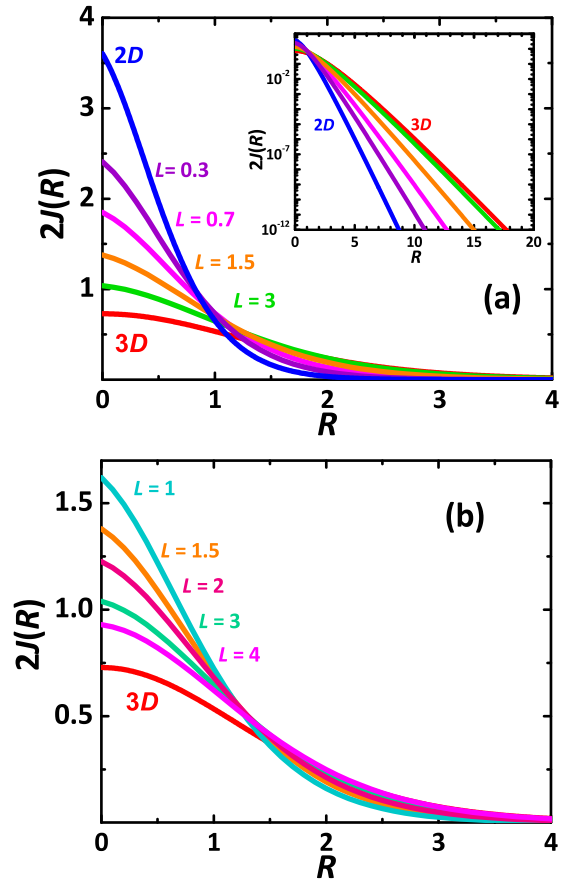

FIG. 6. (a) Interpolated exchange energy $2J(R)$ for the L values shown in Fig. 1, as a function of the distance R between two donor-bound electrons, centered inside the QW. The curves noted 2D and 3D correspond to the interpolated $2J(R)$ laws in 2D and in 3D, respectively, see Eqs. (15). Inset: semilogarithmic representation of the same data, for a larger range of R. (b) Interpolated exchange energy $2J(R)$ for $L = 1,\ 1.5,\ 2,\ 3,\ 4$, and 3D.

As a special case, we recalculated the interpolated formulas in 3D and 2D following our procedure. We found

$$2J_{3D}(R) = 0.729(1 + 0.258R^2)^{\frac{5}{4}} \exp[-0.0005R - 1.270R \arctan(0.508R)]; \quad (15a)$$

$$2J_{2D}(R) = 3.604(1 + 1.548R^2)^{\frac{7}{8}} \exp[-0.579R - 2.178R \arctan(1.244R)]. \quad (15b)$$

These interpolated expressions are remarkably close to the ones calculated in Appendix C.

Figure 5 shows the values of the obtained parameters A and γ, as a function of the QW thickness L; monotonous evolutions of A and γ can be observed between the 2D ($L \to 0$) and 3D ($L \to \infty$) cases. For $L \geqslant 6$, the A and γ values are very close to the values at 3D. In Fig. 6, we plotted the interpolated exchange energy $2J(R)$ for several values of

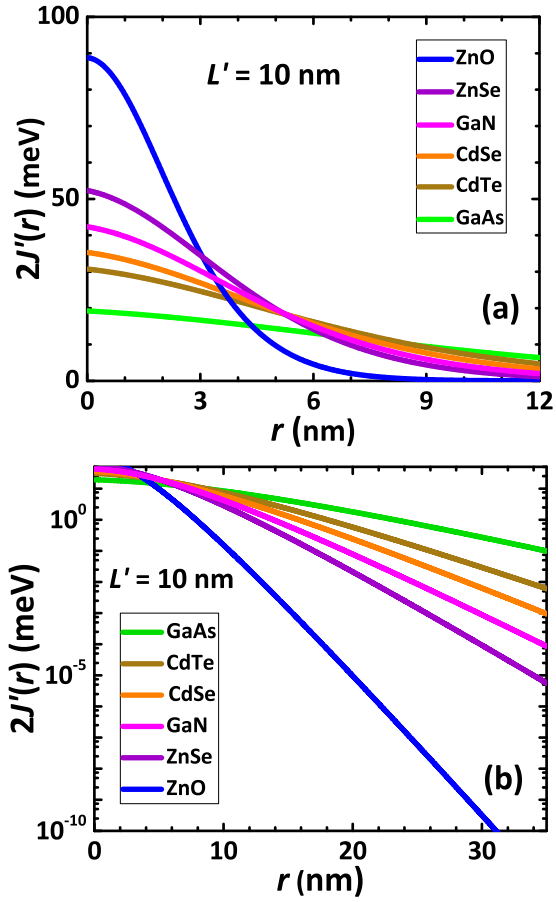

FIG. 7. Electron exchange energy in a common unit of energy, as a function of interdonor distance for several semiconductor materials, at a fixed value of QW thickness $L' = 10$ nm; (a) in linear scales and for small interdonor distances; (b) in semilogarithmic scales and for a larger domain of interdonor distances.

L, as a function of the distance R between two donor-bound electrons, centered inside the QW. Because we consider an infinite QW with a wavefunction completely confined in the QW, our calculations do not describe correctly real systems for $L < 1$. Indeed, the electron wavefunction of thin QWs, for which $L' = La_B^*$ is smaller than a_B^*, is in fact larger than the QW thickness, and then overflows the barrier material which does not represent an infinite barrier for electrons. Figure 6(b) shows with more detail $2J(R)$ for $L \geqslant 1$ and 3D. For $L \leqslant 1$ [see Fig. 6(a)], the exchange energy at very small $R < 1$ shows a maximum for 2D and a minimum for 3D with intermediate values for QWs of different L; however, for $R > 2$ the situation is inverted and the 3D value is larger than the value obtained in a QW or in 2D [see the inset of Fig. 6(a)].

IV. DISCUSSION

The exchange energy $2J(R)$ between two electrons bound to donors, placed in the mid-plane of an infinite QW, has been calculated in units of effective hartree E_h^*, see Sec. III; the distance R between the donors, and the width L of the QW, are expressed in units of effective Bohr radius a_B^* (see Sec. II A). In order to be specific, we present in Figs. 7(a) and 7(b), in common units of energy and of length, the exchange energy $2J'(r) = 2J(R = r/a_B^*) \times E_h^*$ between two donor-bound electrons as a function of the distance between donors, $r = Ra_B^*$, fixing the width of the infinite QW at $L' = 10$ nm, for some usually studied semiconductor materials. The parameters for these compounds are indicated in Table I.

We remark in Fig. 7(a), that the $2J'(0)$ value is larger for materials with a higher effective hartree energy. Indeed, a value close to 100 meV for ZnO is obtained, which is almost five times larger than the $2J'(0)$ value for GaAs. Figure 7(b) shows that, for large interdonor distances, ZnO exhibits also the smallest value of exchange energy, meanwhile GaAs has the largest exchange energy among the materials used for comparison in this figure. We also remark that, for GaAs, the exchange energy of two electrons localized on donors decreases slightly when the interdonor distance increases, meanwhile for ZnO the decrease is much faster. In general, the exchange energy is exponentially sensitive to the distance between donors, and this sensitivity depends also strongly on the effective hartree energy which fixes the extension of the electron wavefunction for a given semiconductor material.

Talking about physical applications, the lowest limit of distance for lithographic techniques, and therefore the closest available distance for qubits, is of the order of tens of nm. When the exchange interaction is the main coupling mechanism between spin qubits, a relatively strong exchange interaction is needed, but also needed is a long spin relaxation time; Linpeng *et al.* [36] have measured in ZnO bulk, with a doping concentration of the order of 10^{17} cm^{-3} (i.e., $r \sim 15$ nm), a relaxation time exceeding 100 ms applying a magnetic field of 2 T, meanwhile Dzhioev *et al.* [22] have found a spin

TABLE I. Values of the different parameters determining the electron exchange energy and the spin relaxation time near the insulator-metal transition, in usually studied semiconductor materials.

Material	Effective mass m^*/m_0	Dielectric constant ϵ_r	Bohr radius a_B^* (nm)	Effective hartree E_h^* (meV)	Energy band gap E_g (eV)	Spin-orbit splitting Δ_{SO} (eV)
ZnO	0.24[a]	7.77[b]	1.71	108	3.44[c]	0.0035[c]
ZnSe	0.145[b]	8.8[d]	3.21	51.0	2.820[e]	0.403[e]
GaN	0.13[f]	9.7[f]	3.95	37.6	3.28[f]	0.02[f]
CdSe	0.11[b]	10.16[d]	4.89	29.0	1.74[g]	0.462[h]
CdTe	0.09[i]	10.31[j]	6.1	23	1.606[e]	0.949[e]
GaAs	0.067[k]	12.35[d]	9.75	12.0	1.519[e]	0.341[e]

[a]Ref. [46]; [b]Ref. [47]; [c]Ref. [48]; [d]Ref. [49]; [e]Ref. [50]; [f]Ref. [51]; [g]Ref. [52]; [h]Ref. [53]; [i]Ref. [54]; [j]Ref. [55]; [k]Ref. [56].

relaxation time of about 100 ns in GaAs for an interdonor distance around 30 nm. Then, when the coupling between two spin qubits is governed by exchange interaction, the choice of the most suitable material is the result of a compromise between large spin relaxation time and large enough exchange interaction.

In Refs. [22–24], it has been shown that the exchange interaction plays an essential role for the spin relaxation of donor-bound electrons near the metal-insulator transition, in which the anisotropic part of the exchange Hamiltonian becomes dominant. Until now, we have only dealt with the isotropic part, but J also appears as a coefficient of the anisotropic terms. The complete exchange Hamiltonian in semiconductor nanostructures is given by [34]

$$\hat{H}_{\rm exc} = 2J[\vec{S}_1 \cdot \vec{S}_2 \cos\gamma + (\vec{d} \cdot \vec{S}_1)(\vec{d} \cdot \vec{S}_2)(1-\cos\gamma) + \vec{d} \cdot (\vec{S}_1 \times \vec{S}_2)\sin\gamma], \quad (16)$$

where $\vec{d}$ is a unit vector and γ is a constant proportional to the distance between the two electrons; $\vec{d}$ and γ both depend on the crystallographic structure. The first anisotropic term in Eq. (16) corresponds to the pseudodipole interaction, and the second one to the Dzyaloshinskii-Moriya (DM) interaction. The magnitude of γ characterizes the strength of the anisotropic part; for small γ, the anisotropic part is dominated by the DM term.

The dopant concentration at which the insulator-metal transition (Mott transition) appears in 3D is fixed by the expression $n_{\rm Mott}^{1/3} a_B^* = 0.25$ [37], which corresponds to the distance $\approx 3a_B^*$ between the donors. The spin relaxation time for localized electrons near the insulator-metal transition, in the insulating phase, is fixed by the anisotropic part of the exchange Hamiltonian. The expression for the spin relaxation time in a QW of thickness L' is then given by [22]

$$\tau_{sa} = \frac{3}{2}\frac{\tau_c}{\gamma^2}, \quad (17)$$

with τ_c the characteristic residence time of an electron on a donor:

$$\tau_c \approx \frac{\hbar}{\xi J'(r)}, \quad (18)$$

in which ξ is a numerical factor of the order of one, approximately equal to 0.8 in the 3D case [22]. In general, for a QW, γ can be written for both zinc-blende (ZB) and wurzite structures as

$$\gamma = 2\pi^2 \frac{\gamma_e b}{E_h^* a_B^{*3}} \left(\frac{a_B^*}{L'}\right)^2 R, \quad (19)$$

with $R = r/a_B^*$, b a parameter equal to 1 or 4 for ZB or wurtzite crystals, respectively, and γ_e is the splitting coefficient related to the Dresselhaus term of the spin-orbit Hamiltonian [38,39]. In the ZB structure, this coefficient $\gamma_e^{\rm ZB}$ is proportional to the spin-orbit constant α (defined in Ref. [40]):

$$\gamma_e^{\rm ZB} = \frac{\alpha\hbar^3}{m^*\sqrt{2m^* E_g}}. \quad (20)$$

The substitution of Eq. (20) in Eq. (19) leads to the expression proposed in Ref. [34]. For a wurzite crystal, the expression for γ_e^W and values for specific materials can be found in Refs. [38,41].

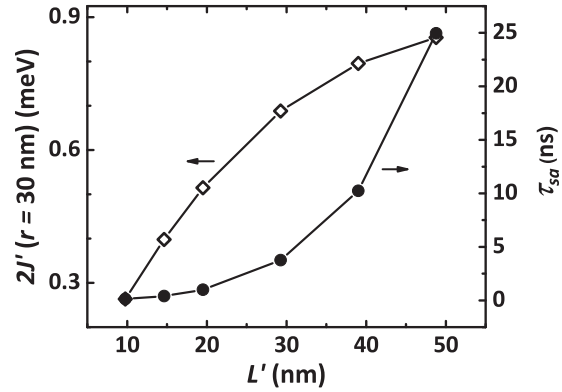

FIG. 8. Electron exchange energy in a common unit of energy (empty diamonds, left axis) and spin relaxation time (full disks, right axis) due to the anisotropic exchange mechanism, for different GaAs QW thicknesses. The distance $r = 30$ nm is fixed between two donor-bound electrons.

For GaAs, one of the most studied materials, the interdonor distance for which the Mott transition appears is around $r_{\rm Mott} \approx 3a_B^* = 30$ nm. In Fig. 8 we show for this material, with $\alpha = 0.073$ [40] and $r = 30$ nm, the calculated electron exchange energy $2J'$ and the spin relaxation time τ_{sa} as a function of the QW thickness. We remark that $2J'(30\,{\rm nm})$ increases as L' increases, and that for $L' \geqslant 30$ nm the exchange energy starts to go to the 3D limit value, meanwhile τ_{sa} increases due to the increase of L'. The upper limit for τ_{sa} is fixed by the 3D case, which we have estimated around 130 ns; as already mentioned, the experimental value measured by Dzhioev *et al.* [22] is around 100 ns.

Spin relaxation properties of GaN and ZnO are less known than those of GaAs. These materials seem very interesting because they show very long spin relaxation and decoherence times. Indeed, Beschoten *et al.* have measured at 5 K and around 220 mT, a spin coherence time of 7 ns for a doping concentration of $3.5 \times 10^{16}\,{\rm cm}^{-3}$ in GaN [42].

In a n-doped ZnO epilayer with concentrations close to the metallic zone, S. Ghosh *et al.* found a spin coherence time of 2 ns at T = 30 K [43]. We now compare this value with the one which can be estimated using the calculated J for a QW. In ZnO, γ_e^W has been calculated to be $0.33\,{\rm eV.Å}^3$ (see Refs. [38,41]), two orders of magnitude smaller than for GaAs. By using the parameters given in Table I, and for a doping concentration in the insulating regime near the Mott transition ($r = 5$ nm), we are then able to estimate a relaxation time $\tau_{sa}^{\rm ZnO} \approx 16$ ns for a QW with a thickness equal to 10 nm. This value is larger than the one obtained for a GaAs QW of the same thickness, $\tau_{sa}^{\rm GaAs} \approx 150$ ps (see Fig. 8), and also larger than the relaxation times measured by Ghosh *et al.* [43] on ZnO epilayers close to the Mott transition (0.5 – 2 ns, for $na_B^{*3} = 0.01 - 0.1$). Nevertheless, the cited experimental values may also depend on spin relaxation processes not discussed in this work, and induced by the optical excitation conditions [24].

TABLE II. Wavefunctions and energies for the 1*s* and 2*s* hydrogenic states in 3D and 2D.

		Wavefunction ϕ	Energy E
3D	1*s*	$\frac{1}{\sqrt{\pi}}\, Z^{3/2} \exp(-Zr)$	$-Z^2/2$
	2*s*	$\frac{1}{2\sqrt{2\pi}}\, Z^{3/2} \exp(-Zr/2)\,[1-Zr/2]$	$-Z^2/8$
2D	1*s*	$\frac{4}{\sqrt{2\pi}}\, Z \exp(-2Z\rho)$	$-2Z^2$
	2*s*	$\frac{4}{3\sqrt{6\pi}}\, Z \exp(-2Z\rho/3)\,[1-4Z\rho/3]$	$-2Z^2/9$

V. CONCLUSION

We obtained a general expression for the exchange energy of two electrons bound to donors placed in the middle of an infinite QW, valid for any interdonor distance and for any QW thickness. This tool allows one, in particular, to calculate the spin relaxation time near the insulator-metal transition in QWs made of widely used II-VI and III-V direct-band-gap materials. Due to the low values of the electron exchange energy and the spin-orbit interaction in ZnO, we deduce that the spin relaxation time in ZnO near the metal-insulator transition should be larger than the one found in GaAs, and then ZnO could be a suitable material for quantum information, provided the entanglement mechanism between spin qubits be different from the electron exchange interaction.

APPENDIX A: 1*s* AND 2*s* HYDROGENIC STATES CENTERED IN AN INFINITE QUANTUM WELL

1. Method

A positive electric charge Ze (e: elementary charge) is at the origin of Cartesian coordinates xyz. The Hamiltonian H of an electron (charge $-e$) in the Coulomb potential of Ze is

$$H = -\frac{\Delta}{2} - \frac{Z}{r}, \tag{A1}$$

where Δ is the Laplacian operator and r is the distance of the electron to the origin. The distances are expressed in units of effective (bulk) Bohr radius a_B^*, and energies in units of effective hartree E_h^* (as mentioned in the beginning of Sec. II A). The 1*s* and 2*s* states in bulk ($r = \sqrt{x^2+y^2+z^2}$) and in 2D ($\rho = \sqrt{x^2+y^2}$) are shown in Table II.

We seek the 1*s* and 2*s* states when the charge Ze is placed in the middle of a QW of thickness L, simply modeled by two infinite barriers located at $z = \pm L/2$; the confinement potential is supposed to be zero inside the QW ($|z| < L/2$). The 1*s* and 2*s* wavefunctions centered within this QW are taken in the following forms:

$$\phi_1(\rho, z) = A_1 \exp(-\alpha_1 r) \cos\left(\pi \frac{z}{L}\right), \tag{A2a}$$

$$\phi_2(\rho, z) = A_2 \exp(-\alpha_2 r)\,[1-\alpha_3 r] \cos\left(\pi \frac{z}{L}\right), \tag{A2b}$$

where $r = \sqrt{\rho^2+z^2}$. The postulated $\cos(\pi z/L)$ envelope function is a single sinusoid arch, and ensures that the wavefunctions $\phi_j(\rho, z)$, $j = 1$ or 2, vanish at the boundaries of the QW. The dependences on r of both ϕ_j respect the ones which are found in the 2D ($L \to 0$) and 3D ($L \to \infty$) limits. In the following of this Appendix, the prefactors A_j are fixed by normalization; $\phi_1(\rho, z)$ and its energy E_1 are first determined by means of the variational method; afterwards, using the 2*s*-1*s* orthogonality and the variational method, $\phi_2(\rho, z)$ and its energy E_2 are obtained.

2. 1*s* state

The normalization condition of the $\phi_1(\rho, z)$ wavefunction gives

$$A_1^{\,2} = \frac{{\alpha_1}^3}{\pi\, N(\alpha_1 L)}, \tag{A3a}$$

with

$$N(X) = 1 - \frac{\pi^2}{X^2+\pi^2} + \frac{\pi^4/2}{[X^2+\pi^2]^2} - \frac{\pi^2}{4}\left(\frac{X+4}{X^2+\pi^2} - \frac{2\pi^2}{[X^2+\pi^2]^2}\right) e^{-X}. \tag{A3b}$$

The forms of the normalization factors of the 3D and 2D 1*s* wavefunctions can be retrieved from this expression: $A_1 \to \alpha_1^{3/2}/\sqrt{\pi}$ for $L \to \infty$, and $A_1\sqrt{L/2} \to \alpha_1\sqrt{2/\pi}$ for $L \to 0$.

The parameter α_1 is obtained by minimization of the mean energy $\tilde{E}_1 = \langle\phi_1|H|\phi_1\rangle$, which is the sum of a kinetic term (possessing, after calculation, a remarkably simple form):

$$\langle\phi_1| -\frac{\Delta}{2} |\phi_1\rangle = \frac{\alpha_1^2}{2} + \frac{\pi^2}{2L^2}, \tag{A4}$$

and a potential term due to the Coulomb interaction:

$$\langle\phi_1| -\frac{Z}{r} |\phi_1\rangle = -\,Z\,\alpha_1\,\frac{C(\alpha_1 L)}{N(\alpha_1 L)}, \tag{A5a}$$

with

$$C(X) = 1 - \frac{1}{2}\,\frac{\pi^2}{X^2+\pi^2}(1+e^{-X}). \tag{A5b}$$

Defining $g(X) = XC(X)/N(X)$, which is a smooth function close to the identity [$g(X) \approx X$], the minimum of $\tilde{E}_1$ is found to be reached when α_1 is solution of the equation

$$\frac{\alpha_1 L}{g'(\alpha_1 L)} = Z\,L. \tag{A6}$$

After a numerical determination of the derivative $g'(X)$ of the function $g(X)$, the left-hand side of the above equation can be calculated for a value of the parameter $\alpha_1 L$. One then obtains the thickness L for which the starting parameter $\alpha_1 L$ corresponds to the minimum of $\tilde{E}_1$; finally, the associated α_1 value is calculated through $\alpha_1 = (\alpha_1 L)/L$, and the energy E_1 of ϕ_1 by substitution of α_1 in the expression for $\tilde{E}_1$. The procedure can be repeated for any starting parameter $\alpha_1 L$, and then allows one to get α_1 and E_1, and also A_1, as a function of the thickness L of the QW, as shown in Fig. 9 for $Z = 1$ and $Z = 2$. One can remark that parameter $\alpha_1(Z = 1)$ for thickness L coincides with $\alpha_1(Z)/Z$ for thickness ZL. The prefactor A_1 goes to $\sqrt{Z^3/\pi}$ (3D limit) for $L \gg 1$, and behaves as $4Z/\sqrt{\pi L}$ for very small L [see Figs. 9(a) and

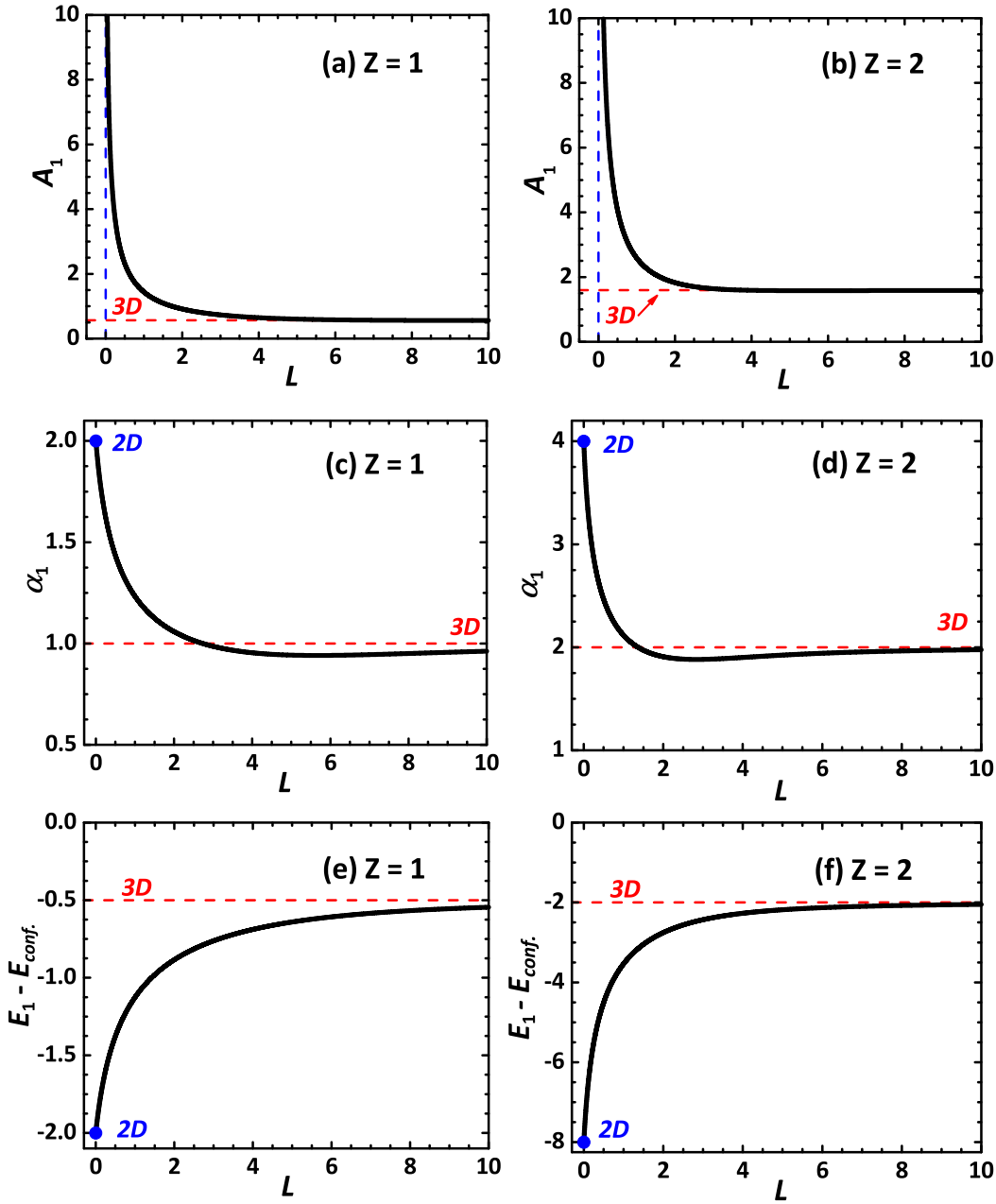

FIG. 9. Parameters A_1 and α_1 of the ϕ_1 wavefunction, and its energy E_1, as a function of the thickness L of the QW (thick continuous curves); the thin red dashed lines correspond to the 3D case. (a), (b): A_1 vs L for $Z = 1$, $Z = 2$. (c), (d): α_1 vs L for $Z = 1$, $Z = 2$. (e), (f): $E_1 - E_{\text{conf}}$ vs L for $Z = 1$, $Z = 2$, where $E_{\text{conf}} = \pi^2/2L^2$.

9(b)]. The parameter α_1 goes to Z (3D limit) for $L \gg 1$, and to $2Z$ (2D limit) for vanishing L [see Figs. 9(c) and 9(d)]. For decreasing values of L, the extension of the ϕ_1 wavefunction first inflates slightly in the xy plane (α_1 becoming a little smaller than Z), and secondly globally shrinks for smaller values of L. The energy E_1, when considered by reference to the confinement energy $E_{\text{conf}} = \pi^2/2L^2$, increases monotonically with L from $-2Z^2$ (2D value) to $-Z^2/2$ (3D value) [see Figs. 9(e) and 9(f)].

3. 2*s* state

The orthogonality condition between the $\phi_1(\rho, z)$ and $\phi_2(\rho, z)$ wavefunctions implies the following relationship between α_1, α_2, and α_3:

$$\alpha_3 = \beta \frac{N(\beta L)}{N(\beta L) + M(\beta L)}, \tag{A7a}$$

with $\beta = \frac{\alpha_1+\alpha_2}{2}$ and

$$M(X) = \frac{1}{2} - \frac{3\pi^2/2}{X^2+\pi^2} + \frac{9\pi^4/4}{[X^2+\pi^2]^2} - \frac{\pi^6}{[X^2+\pi^2]^3} - \frac{\pi^2}{4}\left(\frac{1}{2} + \frac{3X+6-\pi^2/2}{X^2+\pi^2} - \pi^2\frac{2X+9}{[X^2+\pi^2]^2} + \frac{4\pi^4}{[X^2+\pi^2]^3}\right)e^{-X}. \tag{A7b}$$

The relationships between α_1, α_2 and α_3 in 3D and in 2D can be retrieved as limiting cases of the above expressions: $\alpha_3 \to (\alpha_1+\alpha_2)/3$ when $L \to \infty$ and $\alpha_3 \to (\alpha_1+\alpha_2)/2$ when $L \to 0$.

The normalization condition of the $\phi_2(\rho, z)$ wavefunction gives

$$A_2^2 = \frac{\alpha_2^3}{\pi}\left\{N(\alpha_2 L)\left[1 - 2\,\frac{\alpha_3}{\alpha_2} + \frac{3}{2}\frac{\alpha_3^2}{\alpha_2^2}\right] + M(\alpha_2 L)\left[-2\,\frac{\alpha_3}{\alpha_2} + \frac{3}{2}\frac{\alpha_3^2}{\alpha_2^2}\right] + \frac{1}{8}Q(\alpha_2 L)\frac{\alpha_3^2}{\alpha_2^2}\right\}^{-1}, \tag{A8a}$$

with

$$Q(X) = 3 + 3X^4\frac{X^4 - 6\pi^2X^2 + \pi^4}{[X^2+\pi^2]^4} - \frac{\pi^2}{2}\left(\frac{X^3}{X^2+\pi^2} + 3X^2\frac{3X^2+\pi^2}{[X^2+\pi^2]^2} + 6X\frac{6X^4+3\pi^2X^2+\pi^4}{[X^2+\pi^2]^3} + 6\frac{10X^6+5\pi^2X^4+4\pi^4X^2+\pi^6}{[X^2+\pi^2]^4}\right)e^{-X}. \tag{A8b}$$

The energy E_2 is obtained as the minimum of the mean energy $\tilde{E}_2 = \langle\phi_2|H|\phi_2\rangle$, which only depends on α_2 (α_1 is known, α_3 is a function of α_1 and α_2). $\tilde{E}_2$ is the sum of a kinetic term:

$$\langle\phi_2|-\frac{\Delta}{2}|\phi_2\rangle = \frac{1}{4}\left(\frac{\pi A_2^2}{\alpha_2^3}\right)\left\{\frac{\pi^2}{L^2}\left[Q_1(\alpha_2 L) - \frac{\alpha_3}{\alpha_2}Q_2(\alpha_2 L) + \frac{\alpha_3^2}{4\alpha_2^2}Q_3(\alpha_2 L)\right] + 2\alpha_2^2 C(\alpha_2 L) + \alpha_3^2\,[N(\alpha_2 L) + 2M(\alpha_2 L)] + 2\alpha_2\alpha_3[C(\alpha_2 L) - 2N(\alpha_2 L)]\right\}, \tag{A9a}$$

with

$$Q_1(X) = 1 - \left(1 + \frac{X}{2}\right)e^{-X} \tag{A9b}$$

$$Q_2(X) = 3 - \left(3 + 2X + \frac{1}{2}X^2\right)e^{-X} \tag{A9c}$$

$$Q_3(X) = 12 - \left(12 + 9X + 3X^2 + \frac{1}{2}X^3\right)e^{-X}, \tag{A9d}$$

and a potential term due to the Coulomb interaction:

$$\langle\phi_2|-\frac{Z}{r}|\phi_2\rangle = -Z\,\frac{\pi A_2^2}{\alpha_2^2}\left\{C(\alpha_2 L) + N(\alpha_2 L) \times\left[-2\frac{\alpha_3}{\alpha_2} + \frac{\alpha_3^2}{\alpha_2^2}\right] + M(\alpha_2 L)\frac{\alpha_3^2}{\alpha_2^2}\right\}. \tag{A10}$$

Finding the parameter α_2 [and consequently α_3, with Eq. (A7a)] which minimizes $\tilde{E}_2$ (at given L) requires a long numerical procedure, which is in contrast with the much easier work needed for the minimization of $\tilde{E}_1$. Figure 10 shows A_2, α_2, α_3 and E_2 concerning the ϕ_2 wavefunction, for different values of the thickness L, with $Z = 1$ and $Z = 2$: A_2 and α_2 behave with L just as A_1 and α_1 do; α_3 monotonically decreases with L; however, E_2, considered by reference to the confinement energy $E_{\rm conf} = \pi^2/2L^2$, goes with L from $-2Z^2/9$ (2D value) to $-Z^2/8$ (3D value) but nonmonotonically [see Figs. 10(e) and 10(f)].

APPENDIX B: EXCHANGE ENERGY OF A "HELIUM ATOM" CENTERED IN AN INFINITE QUANTUM WELL

1. Exact results in 3D

The nonrelativistic energies of the (singlet) $(1s)^2$ ground state and of the first-excited triplet $1s2s$ state of the helium atom in 3D are known with an excellent precision: in Ref. [44] they are calculated with 20 significant digits. We only write here the first of them:

$$E_S^{\rm exact} = -2.9037, \quad E_A^{\rm exact} = -2.1752, \tag{B1a}$$

in units of effective hartree (see the beginning of Sec. II A). The subscript S, or A, recalls that the orbital part of the state is symmetric, or antisymmetric, under permutation of both electrons of the atom. The exchange energy $2J_0 = E_A - E_S$ is then exactly, in 3D:

$$2J_0^{\rm exact} = 0.7285. \tag{B1b}$$

2. Exact results in 2D

In 2D, the nonrelativistic energies of the $(1s)^2$ ground state and the first-excited triplet $1s2s$ state of the helium atom are also known with a very good accuracy: in Ref. [45] they are calculated with 13 significant digits. We write here the first of them:

$$E_S^{\rm exact} = -11.900, \quad E_A^{\rm exact} = -8.296, \tag{B2a}$$

in units of effective hartree. The exchange energy is then exactly, in 2D:

$$2J_0^{\rm exact} = 3.604. \tag{B2b}$$

3. Calculation of $2J_0$ in an infinite quantum well

The Hamiltonian describing both electrons in a helium atom is written as

$$\hat{H} = -\frac{\Delta_1}{2} - \frac{\Delta_2}{2} - \frac{Z}{r_1} - \frac{Z}{r_2} + \frac{1}{r_{12}}, \tag{B3}$$

where Δ_j is the Laplacian operator acting on electron j ($j = 1$ or 2) and r_j is the distance of electron j to the origin of the coordinates, where the $Z = 2$ nucleus is located; $r_{12} = |\vec{r}_2 - \vec{r}_1|$ is the distance between the electrons.

The ground energy E_S of the "helium atom" centered in a QW with infinite barriers is determined here by the variational method. The ground-state wavefunction $\Psi_S(\vec{r}_1, \vec{r}_2)$ of the pair of electrons 1 and 2 is taken as the product of two one-electron $1s$ wavefunctions: $\Psi_S(\vec{r}_1, \vec{r}_2) = \phi_1(\vec{r}_1)\phi_1(\vec{r}_2)$; the mean energy $\tilde{E}_S = \langle\Psi_S|\hat{H}|\Psi_S\rangle$ is studied as a function of the

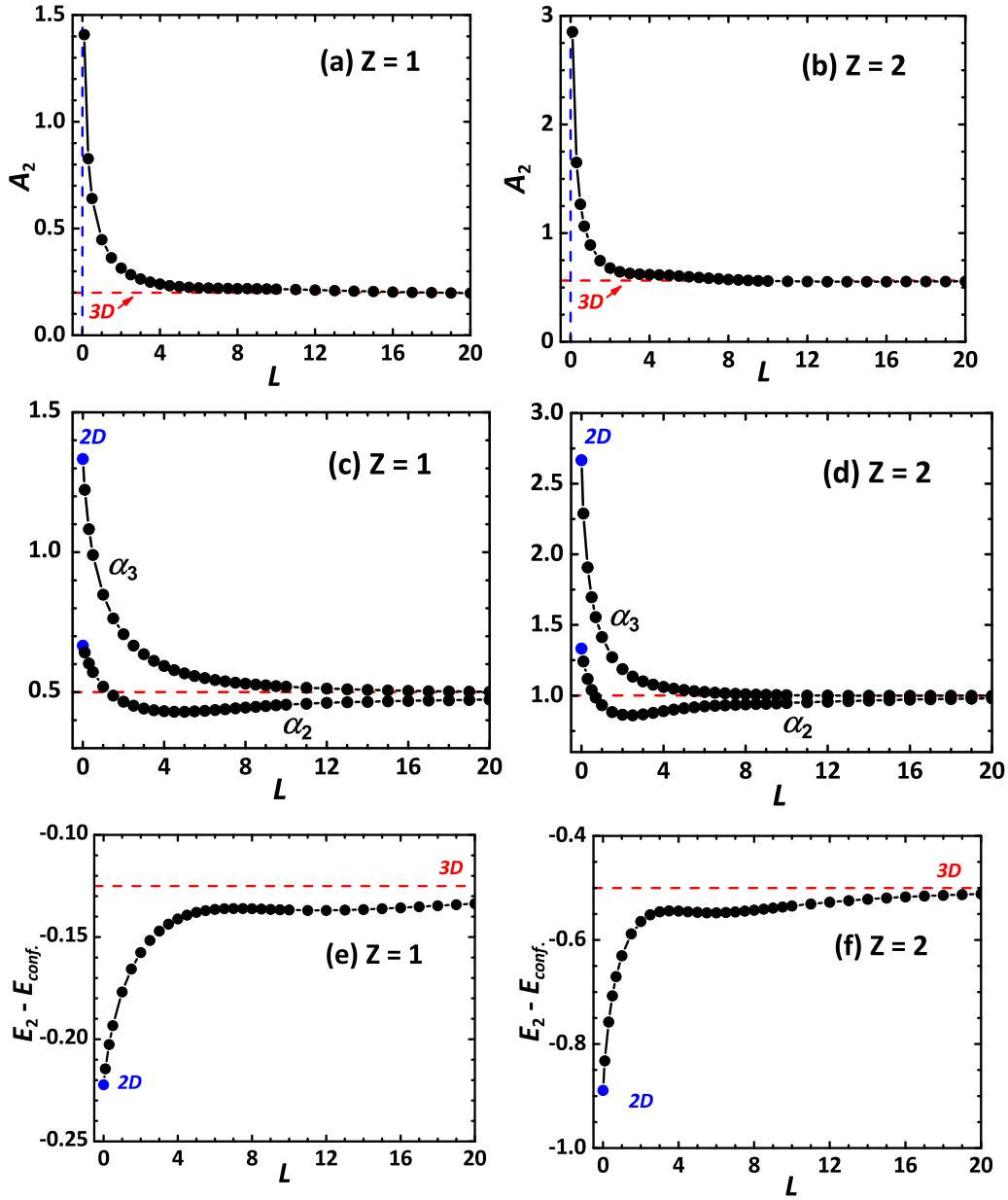

FIG. 10. Parameters A_2, α_2 and α_3 of the ϕ_2 wavefunction, and its energy E_2, as a function of the thickness L of the QW (circular dots; continuous curves: guides for the eyes); the thin red dashed lines correspond to the 3D case. (a), (b): A_2 vs L for $Z = 1$, $Z = 2$. (c), (d): α_2 and α_3 vs L for $Z = 1$, $Z = 2$. (e), (f): $E_2 - E_{\rm conf}$ vs L for $Z = 1$, $Z = 2$ ($E_{\rm conf} = \pi^2/2L^2$).

parameter α_1, which now can vary (see Appendix A 1 for the definitions of ϕ_1 and α_1), and its minimum is taken for the value of E_S. $\tilde{E}_S$ is the sum of a kinetic term:

$$\langle\Psi_S|-\frac{\Delta_1}{2}-\frac{\Delta_2}{2}|\Psi_S\rangle = \alpha_1^2 + \frac{\pi^2}{L^2}, \tag{B4a}$$

a potential term due to the Coulomb interaction of the electrons with the $Z = 2$ nucleus:

$$\langle\Psi_S|-\frac{2}{r_1}-\frac{2}{r_2}|\Psi_S\rangle = -4\,\alpha_1\,\frac{C(\alpha_1 L)}{N(\alpha_1 L)} \tag{B4b}$$

[$N(X)$ and $C(X)$: see Appendix A], and a Coulomb electron-electron term:

$$\langle\Psi_S|\frac{1}{r_{12}}|\Psi_S\rangle = 32\pi\int_0^\infty\int_0^\infty \frac{\rho_q d\rho_q dz_q}{\rho_q^2+z_q^2}\left[\int_0^{\frac{L}{2}} dz\cos(z_q z)\int_0^\infty d\rho\;\rho\;J_0(\rho_q\rho)\,\phi_1(\rho,z)^2\right]^2, \tag{B4c}$$

expressed using the fact that $1/r$ is the inverse Fourier transform of $4\pi/q^2$ [$J_0(x)$ is the Bessel function of first kind and of zeroth order]. This integral is calculated numerically.

The first-excited energy E_A of the "helium atom" centred in a QW with infinite barriers is determined perturbatively here: the electron-electron interaction $1/r_{12}$ is treated as a small correction to the state $\Psi_A(\vec{r}_1,\vec{r}_2) = [\phi_1(\vec{r}_1)\phi_2(\vec{r}_2) - \phi_2(\vec{r}_1)\phi_1(\vec{r}_2)]/\sqrt{2}$ of energy $E_1 + E_2$ (ϕ_1, ϕ_2, E_1, and E_2 are given in Appendix A). The energy E_A is of the form $E_A = E_1 + E_2 + \Delta E$, the corrective term being $\Delta E = \langle\Psi_A|1/r_{12}|\Psi_A\rangle$; ΔE is the sum of a direct term:

$$\iint d^3r_1 d^3r_2 \, \frac{\phi_1(\vec{r}_1)^2\phi_2(\vec{r}_2)^2}{r_{12}} = 32\pi \int_0^\infty \int_0^\infty \frac{\rho_q d\rho_q dz_q}{\rho_q^2 + z_q^2} \left[\int_0^{\frac{L}{2}} dz \cos(z_q z) \int_0^\infty d\rho \; \rho \; J_0(\rho_q \rho) \; \phi_1(\vec{r})^2\right] \times \left[\int_0^{\frac{L}{2}} dz \cos(z_q z) \int_0^\infty d\rho \; \rho \; J_0(\rho_q \rho) \; \phi_2(\vec{r})^2\right], \tag{B5a}$$

and an exchange term:

$$\iint d^3r_1 d^3r_2 \, \frac{\phi_1(\vec{r}_1)\phi_2(\vec{r}_2)\phi_2(\vec{r}_1)\phi_1(\vec{r}_2)}{r_{12}} = 32\pi \int_0^\infty \int_0^\infty \frac{\rho_q d\rho_q dz_q}{\rho_q^2 + z_q^2} \left[\int_0^{\frac{L}{2}} dz \cos(z_q z) \int_0^\infty d\rho \; \rho \; J_0(\rho_q \rho) \phi_1(\vec{r}) \; \phi_2(\vec{r})\right]^2. \tag{B5b}$$

In 3D and in 2D, calculating E_S by the variational method and E_A perturbatively gives satisfactory values (for our purpose) of the exchange energy $2J_0 = E_A - E_S$: we so obtain $2J_0 = -2.124 + 2.848 = 0.724$ in 3D, and $-7.948 + 11.635 = 3.687$ in 2D, which are 0.6% smaller, and 2% larger, than the exact values, respectively. We are then confident that our calculated exchange energies $2J_0$ of a "helium atom" centred in infinite QWs of different thicknesses, possess an uncertainty of the 1% order.

Figure 11 shows our calculated values of the ground energy E_S and first-excited energy E_A, as a function of the thickness L of the QW; the exact values in 2D ($L \to 0$) and in 3D ($L \to \infty$) are also indicated. E_S and E_A monotonically increase with the thickness L, and their difference, which is $2J_0$, monotonically decreases, as shown in Fig. 2.

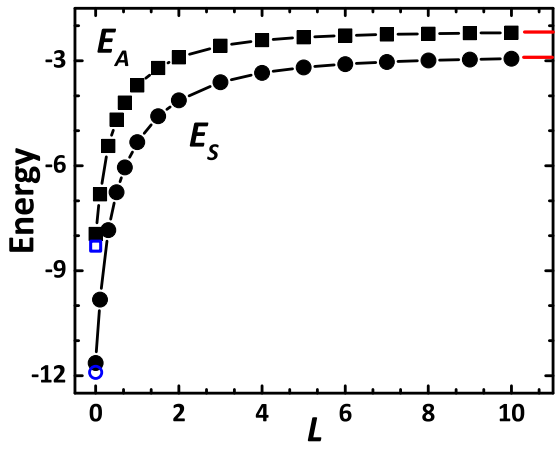

FIG. 11. Ground energy E_S (full disks) and first-excited energy E_A (full squares) of a "helium atom", as a function of the thickness L of the infinite QW; the continuous curves are guides for the eyes. The empty circle and empty square, at $L = 0$, are the exact values in 2D. The exact values in 3D are indicated by two horizontal red segments, on the right of the graph.

APPENDIX C: NEW INTERPOLATED FORMULAS FOR THE 3D AND 2D EXCHANGE ENERGIES

Section III A described the procedure of Ref. [32] to build an interpolated expression of the exchange energy $2J(R)$ in 3D and 2D. In Eq. (14), in which A is the only remaining free parameter, it is possible, alternatively, to impose that, for $R \gg 1$, the interpolated $2J(R)$ be in coincidence with the standard asymptotic form (11). We then obtain the following expression for A:

$$A = (C/2J_0)^{1/\beta}/\mathrm{e}. \tag{C1}$$

So we can propose new interpolated formulas for the exchange energy $2J(R)$ in 3D and 2D, using values of $2J_0$ which are, nowadays, known with very good accuracy (see Appendix B):

$$2J_{3D}(R) = 0.729\,(1 + 0.259R^2)^{\frac{5}{4}} \exp[-0.003R - 1.271R \arctan(0.509R)]; \tag{C2a}$$

$$2J_{2D}(R) = 3.604\,(1 + 1.549R^2)^{\frac{7}{8}} \exp[-0.579R - 2.178R \arctan(1.245R)]. \tag{C2b}$$

These expressions give $2J(R)$ values close to the corresponding ones of Ref. [32] for R of the order the order of unity, and are more satisfactory, by construction, for large values of R.

APPENDIX D: CORRELATION FUNCTION FOR THE 3D CASE

In Sec. II B, we have found that, in the case of an infinite QW, the correlation function satisfies

$$\chi(\vec{r}_1,\vec{r}_2) = \chi_{3D}(\vec{r}_1,\vec{r}_2)^{1/\alpha_1},$$

where $\chi_{3D}(\vec{r}_1,\vec{r}_2)$ is given by the expression [30]:

$$\chi_{3D}(\vec{r}_1,\vec{r}_2) = \frac{2a(2a + x_1 + x_2)}{(a - x_1)(a + x_2)} \exp\left(-\frac{a + x_1}{2a}\right) \times \left\{\frac{\sqrt{(x_1 - x_2)^2 + \rho_{12}^2} + x_2 - x_1}{\sqrt{(2a + x_1 + x_2)^2 + \rho_{12}^2} + 2a + x_1 + x_2}\right\}^{1/2}$$

for $x_1 + x_2 < 0$, and

$$\chi_{3D}(\vec{r}_1, \vec{r}_2) = \frac{2a(2a - x_1 - x_2)}{(a - x_1)(a + x_2)} \exp\left(-\frac{a - x_2}{2a}\right) \left\{ \frac{\sqrt{(x_1 - x_2)^2 + \rho_{12}^2} + x_2 - x_1}{\sqrt{(2a - x_1 - x_2)^2 + \rho_{12}^2} + 2a - x_1 - x_2} \right\}^{1/2}$$

for $x_1 + x_2 > 0$; the notation $\rho_{12} = \sqrt{(y_1 - y_2)^2 + (z_1 - z_2)^2}$ is employed.

[1] D. P. DiVincenzo, Science **270**, 255 (1995).
[2] M. A. Nielsen and I. L. Chuang, *Quantum Computation and Quantum Information* (Cambridge University Press, Cambridge, 2000).
[3] J. Clarke and F. K. Wilhelm, Nature (London) **453**, 1031 (2008).
[4] M. H. Devoret and R. J. Schoelkopf, Science **339**, 1169 (2013).
[5] R. Hanson and D. D. Awschalom, Nature (London) **453**, 1043 (2008).
[6] J. J. L. Morton and B. W. Lovet, Annu Rev. Condens. Matter Phys. **2**, 189 (2011).
[7] D. Loss and D. P. DiVincenzo, Phys. Rev. A **57**, 120 (1998).
[8] G. Buckard, D. Loss, and D. P. DiVincenzo, Phys. Rev. B **59**, 2070 (1999).
[9] B. E. Kane, Nature (London) **393**, 133 (1998).
[10] P. M. Koenraad and M. E. Flatté, Nat. Mater. **10**, 91 (2011).
[11] F. Jelezko and J. Wrachtrup, Phys. Status Solidi A **203**, 3207 (2006).
[12] M. W. Doherty, N. B. Manson, P. Delaney, F. Jelezko, J. Wrachtrup, and L. C. L. Hollenberg, Phys. Rep. **528**, 1 (2013).
[13] W. F. Koehl, B. B. Buckley, F. J. Heremans, G. Calusine, and D. D. Awschalom, Nature (London) **479**, 84 (2011).
[14] J. M. Kikkawa and D. D. Awschalom, Phys. Rev. Lett. **80**, 4313 (1998).
[15] R. Vrijen, E. Yablonovitch, K. Wang, H. W. Jiang, A. Balandin, V. Roychowdhury, T. Mor, and D. Di Vincenzo, Phys. Rev. A **62**, 012306 (2000).
[16] P. H. Kasai, Phys. Rev. **130**, 989 (1963).
[17] H. Horn, A. Balocchi, X. Marie, A. Bakin, A. Waag, M. Oestreich, and J. Hübner, Phys. Rev. B **87**, 045312 (2013).
[18] J. Tribollet, E. Aubry, G. Karczewski, B. Sermage, F. Bernardot, C. Testelin, and M. Chamarro, Phys. Rev. B **75**, 205304 (2007).
[19] M. Chamarro, F. Bernardot, and C. Testelin, J. Phys: Condens Matter **19**, 445007 (2007).
[20] K. De Greve, S. M. Clark, D. Sleiter, K. Sanaka, T. D. Ladd, M. Panfilova, A. Pawlis, K. Lischka, and Y. Yamamoto, Appl. Phys. Lett. **97**, 241913 (2010).
[21] Y. M. Kim, D. Sleiter, K. Sanaka, D. Reuter, K. Lischka, Y. Yamamoto, and A. Pawlis, Current Appl. Phys. **14**, 1234 (2014).
[22] R. I. Dzhioev, K. V. Kavokin, V. L. Korenev, M. V. Lazarev, B. Ya. Meltser, M. N. Stepanova, B. P. Zakharchenya, D. Gammon, and D. S. Katzer, Phys. Rev. B **66**, 245204 (2002).
[23] R. I. Dzhioev, V. L. Korenev, I. A. Merkulov, B. P. Zakharchenya, D. Gammon, Al. L. Efros, and D. S. Katzer, Phys. Rev. Lett. **88**, 256801 (2002).
[24] K. V. Kavokin, Semicond. Sci. Technol. **23**, 114009 (2008).
[25] A. Imamoglu, D. D. Awschalom, G. Burkard, D. P. DiVincenzo, D. Loss, M. Sherwin, and A. Small, Phys. Rev. Lett. **83**, 4204 (1999).
[26] W. Yao, R B. Liu, and L. J. Sham, Phys. Rev. Lett. **95**, 030504 (2005).
[27] C. Piermarocchi, P. Chen, L. J. Sham, and D. G. Steel, Phys. Rev. Lett. **89**, 167402 (2002).
[28] E. Pazy, E. Biolatti, T. Calarco, I. D'Amico, P. Zanardi, F. Rossi, and P. Zoller, Europhys. Lett. **62**, 175 (2003).
[29] D. P. DiVincenzo, D. Bacon, J. Kempe, G. Burkard, K. B. Whaley, Nature (London) **408**, 339 (2000).
[30] L. P. Gor'kov and L. P. Pitaevskii, Dokl. Akad. Nauk SSSR **151**, 822 (1963) [Sov. Phys. Doklady **8**, 788 (1964)].
[31] C. Herring and M. Flicker, Phys. Rev. **134**, A362 (1964).
[32] I. V. Ponomarev, V. V. Flambaum, and A. L. Efros, Phys. Rev. B **60**, 5485 (1999).
[33] I. V. Ponomarev, V. V. Flambaum, and A. L. Efros, Phys. Rev. B **60**, 15848 (1999).
[34] K. V. Kavokin, Phys. Rev. B **69**, 075302 (2004).
[35] W. Heitler and F. London, Z. Phys. **44**, 455 (1927).
[36] X. Linpeng, M. L. K. Viitaniemi, A. Vishnuradhan, Y. Kozuka, C. Johnson, M. Kawasaki, and K-M C. Fu, arXiv:1802.03483v3 (2018).
[37] N. F. Mott, *Metal Insulator Transitions* (Taylor and Francis, London, 1990).
[38] J. Y. Fu and M. W. Wu, J. Appl. Phys. **104**, 093712 (2008).
[39] N. J. Harmon, W. O. Putikka, and R. Joynt, Phys. Rev. B **79**, 115204 (2009).
[40] G. E. Pikus and A. M. Titkov, in *Optical Orientation*, edited by F. Meier and B. P. Zachachrenya (North-Holland, Amsterdam, 1984).
[41] L. C. Lew Yan Voon, M. Willatzen, M. Cardona, and N. E. Christensen, Phys. Rev. B **53**, 10703 (1996).
[42] B. Beschoten, E. Johnston-Halperin, D. K. Young, M. Poggio, J. E. Grimaldi, S. Keller, S. P. DenBaars, U. K. Mishra, E. L. Hu, and D. D. Awschalom, Phys. Rev. B **63**, 121202 (2001).
[43] S. Ghosh, V. Sih, W. H. Lau, and D. D. Awschalom, Appl. Phys. Lett. **86**, 232507 (2005).
[44] D. T. Aznabayev, A. K. Bekbaev, I. S. Ishmukhamedov, and V. I. Korobov, Phys. Part. Nucl. Lett. **12**, 689 (2015).
[45] L. Hilico, B. Grémaud, T. Jonckheere, N. Billy, and D. Delande, Phys. Rev. A **66**, 022101 (2002).
[46] M. Oshikiri, Y. Imanaka, F. Aryasetiawan, and G. Kido, Physica B **298**, 472 (2001).
[47] N. Ashkenov *et al.*, J. Appl. Phys. **93**, 126 (2003).
[48] W. J. Fana, J. B. Xiab, P. A. Agus, S. T. Tan, S. F. Yu, and X. W. Sun, J. Appl. Phys. **99**, 013702 (2006).

[49] R. Geick, C. H. Perry, and S. S. Mitra, J. Appl. Phys. **37**, 1994 (1966).
[50] H. Mayer and U. Rössler, Solid State Commun. **87**, 81 (1993).
[51] Bougrov *et al.*, in *Properties of Advanced Semiconductor Materials GaN, AlN, InN, BN, SiC, SiGe*, edited by M. E. Levinshtein, S. L. Rumyantsev, and M.S. Shur (Wiley, New York, 2001).
[52] S. Ninomiya and S. Adachi, J. Appl. Phys. **78**, 4681 (1995).
[53] H. Fu, L.W. Wang, and A. Zunger, Phys. Rev. B **59**, 5568 (1999).
[54] I. Hernández-Calderón, in *II-VI Semiconductor Materials and their Applications*, edited by M. C. Tamargo (Taylor and Francis, New York, 2002).
[55] I. Strzalkowski, S. Joshi, and C. R. Crowell, Appl. Phys. Lett. **28**, 350 (1976).
[56] W. Nakwaski, Physica B **210**, 1 (1995).